

## Research Article

# Rapid construction and intrinsic mechanism of host-guest room temperature phosphorescence systems

Weirao Ji <sup>a,1</sup>, Yupeng Zhao <sup>b,1</sup>, Jianmei Guo <sup>a</sup>, Lei Ma <sup>b,\*\*</sup>, Yongtao Wang <sup>a,\*</sup>

<sup>a</sup> College of Chemistry and Bioengineering, Guilin University of Technology, Guilin, 541004, PR China

<sup>b</sup> Tianjin International Center for Nanoparticles and Nanosystem, Tianjin University, Tianjin, 300072, PR China

## ABSTRACT

The construction of small molecule host-guest room temperature phosphorescence (RTP) systems usually involved melting, which required low melting point and excellent thermostability for host materials, limiting the selection range of host materials. Here, 2-(3-(9H-carbazol-9-yl)benzyl)malononitrile (L-DCN) and 2-(3-(5H benzo[b]carbazol-5-yl)benzyl)malononitrile (m-BCzCN) were prepared by self-made carbazole and 2-naphthylamine. Based on the side chain with multiple cyanide groups and similar molecular structures between L-DCN and m-BCzCN, crystallization ability of L-DCN and the compatibility between L-DCN and m-BCzCN were significantly enhanced. Thereby, rapid construction of long-lived host-guest RTP systems could be achieved by organic solvent dissolution and rapid evaporation of L-DCN and m-BCzCN. To explore the effects of trace carbazole impurities, DCN with the same structure with L-DCN was prepared by choosing commercial carbazole. Moreover, RTP performance of L-DCN was further optimized by host-guest doping and tuning the mass ratios between polyvinyl alcohol (PVA) and L-DCN. Compared with crystals DCN, RTP performance of 1 % L-DCN@PVA was not significantly improved, but 1 % L-DCN/m-BCzCN constructed by dissolution and rapid volatilization showed almost equivalent afterglow lifetimes, with RTP lifetimes of 435.37 ms and quantum yield ( $\Phi_p$ ) of 0.06, achieving the expected goal. Finally, advanced encryptions were successfully constructed based on the different luminescent properties of L-DCN in PVA films at different doping concentrations.

## 1. Introduction

Pure organic room temperature phosphorescent (PORTP) materials have mild reaction conditions [1], low toxicity and price [2–4], large Stokes shift [5], long afterglow lifetime [6], and good biocompatibility [7,8], triggering increasing attention from researchers [9]. However, the weak intersystem crossing (ISC) between singlet ( $S_1$ ) and triplet ( $T_1$ ) states in PORTP materials, as well as the fast non-radiative rate of triplet excitons, make it difficult to achieve efficient room temperature phosphorescence (RTP) emission [10]. In addition, long-lived triplet excitons are highly susceptible to external interference such as molecular vibration, heat, and oxygen [11–15], leading visible RTP only at low temperature (77 K) and in the presence of inert gases [16–18]. Therefore, how to obtain PORTP materials with long lifetime and high quantum yield is an urgent problem that needs to be solved.

To solve the above issues, on the one hand, modifying the molecular skeleton and introducing specific functional groups enhance intermolecular interactions and spin orbit coupling (SOC), and thereby boost ISC and suppress non-radiative deactivation [19]. On the other hand, the guest material was doped into a rigid matrix to suppress non radiative

deactivation, considering the energy level matching and compatibility between the host and guest materials. Currently, host-guest doping has made tremendous progress in RTP due to flexible selectivity of host and guest materials. Of note, some 1H-benzof[f]indole (Bd) and benzocarbazole (Bc) derivatives were designed and synthesized [20], and their doping systems showed excellent RTP [21]. Besides, introducing CN and  $sp^3$ -methylene linkers contributes to enhance intermolecular interactions and ISC according to the reported literatures [22,23]. Inspired by trace impurities in commercial carbazole, CN, and  $sp^3$ -methylene linkers, DCN, L-DCN, and m-BCzCN were prepared (Scheme-1), and their doping systems were constructed and optimized [24].

The results indicate crystals DCN with trace Bd emit yellow afterglow, whose RTP quantum yield ( $\Phi_p$ ), RTP and afterglow lifetimes are 0.15, 874.76 ms and 6 s in turn, while crystals L-DCN show weak green afterglow, corresponding to  $\Phi_p$ , RTP and afterglow lifetimes of 0.05, 342.97 ms, 2 s respectively. By host-guest doping, 1 % L-DCN@PVA film presents blue afterglow, but its  $\Phi_p$  (0.05), RTP (345.34 ms) and afterglow (3 s) lifetimes have not been significantly improved than that of crystals L-DCN. By dissolution and rapid solvent evaporation, 1 % L-DCN/m-BCzCN was obtained at the mass ratio of 100:1 between L-DCN

\* Corresponding author.

\*\* Corresponding author.

E-mail addresses: [lei.ma@tju.edu.cn](mailto:lei.ma@tju.edu.cn) (L. Ma), [wyt\\_shzu@163.com](mailto:wyt_shzu@163.com) (Y. Wang).

<sup>1</sup> Contributed equally.

and m-BCzCN. In contrast, 1 % L-DCN/m-BCzCN shows  $\Phi_p$  of 0.06, long afterglow (5 s) and RTP lifetimes (435.37 ms). By changing the doping concentration of L-DCN in PVA, different doping films show the same fluorescence, but with different afterglow lifetimes, and thereby a set of data encryption was achieved. More importantly, the underlying mechanism behind RTP has been further explored through crystal analysis and theoretical calculations.

## 2. Results and discussion

### 2.1. Photophysical Characterization

According to the previously reported synthetic route [20,21,24], DCN was prepared by using commercial carbazole via two synthesis reactions, whose structure (Figs. S5–16) was characterized by  $^1\text{H}$  and  $^{13}\text{C}$  nuclear magnetic resonance (NMR), high resolution mass spectra (HR-MS), and X-ray single crystal diffraction. Firstly, UV-vis absorption and emission spectra of DCN in DCM solution were examined. DCN exhibited multiple absorption bands at 270–310 nm and 310–350, corresponding to  $\pi-\pi^*$  and  $n-\pi^*$  transitions respectively (Fig. S1a). As the solvent polarity increases from n-hexane to DMSO, UV-vis absorption and emission maxima of DCN show small stokes shifts, indicating weak intramolecular charge transfer effect (ICT), which is consistent with stronger absorption for  $\pi-\pi^*$  transition and  $n-\pi^*$  transition (Fig. S1b).

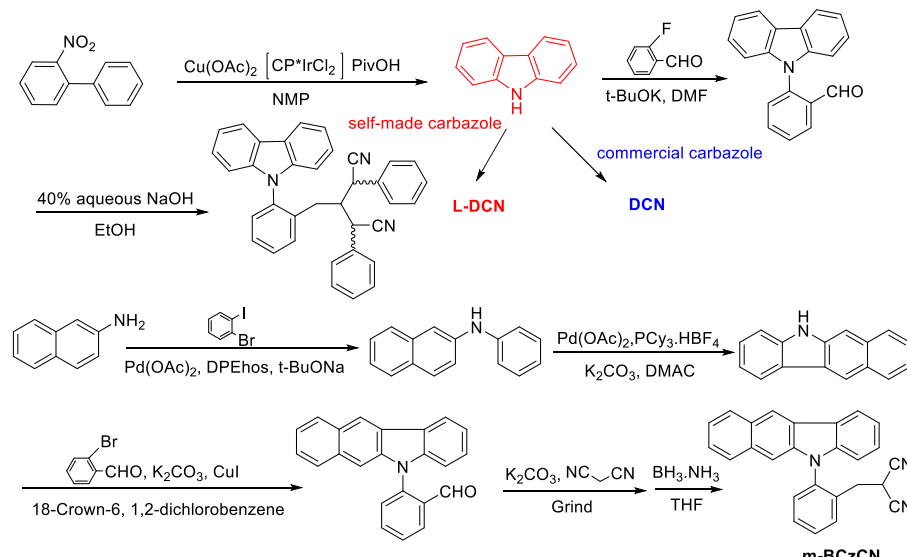
Crystals DCN were obtained by slowly evaporating n-hexane-DCM solution, emitting blue fluorescence under the irradiation of a 365 nm UV lamp. After turning off the UV lamp, crystals DCN emit bright yellow afterglow at room temperature, lasting for 6 s (Fig. 1a). Fluorescence emission maxima of crystals DCN are located at 384 nm, but with multiple RTP peaks at 549 nm, 594 nm, and 650 nm, corresponding to phosphorescence lifetimes of 874.76 ms, 845.21 ms, and 681.05 ms, respectively (Fig. 1b and d). Based on the previous research [25,26], the RTP peaks originate from newly generated charge separated states. To completely eliminate the influence of trace carbazole isomer, L-DCN was synthesized by using self-made carbazole [27–30]. As shown in Fig. 1c and e, fluorescence spectrum of crystals L-DCN is consistent with that of DCN, with emission maxima at 383 nm, but L-DCN only has a phosphorescence peak at 520 nm, with RTP lifetimes of 342.97 ms and weak green afterglow, lasting for 2 s. Obviously, L-DCN is phosphorescence nature, but trace carbazole isomer plays an important role in enhancing RTP performance.

### 2.2. L-DCN@PVA doping system

To enhance RTP performance of L-DCN, L-DCN was doped into polyvinyl alcohol (PVA) matrix at mass fractions of 0.2 %, 1 %, and 5 % respectively. As shown in Fig. 2a, under the irradiation of a 365 nm UV lamp, deep blue fluorescence was observed. After being illuminated for 60 s, light blue afterglow can be observed for 0.2 % L-DCN@ PVA and 1 % L-DCN@ PVA films, but without visible afterglow for 5 % L-DCN@ PVA film, which may be due to ineffectively suppress the rotation and vibration of molecules, as well as the quenching of oxygen at high doping concentrations. Among of the doping films, 1 % L-DCN@PVA film shows the longest afterglow (Fig. 2a), but RTP (345.34 ms) (Fig. 2d) and afterglow (3 s) (Fig. 2a) lifetimes have not been significantly improved for 1 % L-DCN@PVA film than crystals L-DCN, which should be attributed to weak ISC ability for L-DCN. Fluorescence and phosphorescence emission of 1 % L-DCN@PVA are 365 and 494 nm in sequence (Fig. 2c), which are close to fluorescence emission of DCN in various solvents (Fig. S1b) and phosphorescence emission of L-DCN in DCM solution at 77 K (Fig. 2b), indicating that L-DCN is uniformly dispersed in PVA film and presents monomer phosphorescence emission.

### 2.3. L-DCN/m-BCzCN doping systems

By contrast, RTP performance of DCN is significantly better than that of crystals L-DCN and 1 % L-DCN@PVA, once again confirming the superiority of isomer carbazole doping. Thereby, m-BCzCN was prepared, with a similar molecular structure to L-DCN, but with larger molecular conjugation (Scheme-1). By dissolving L-DCN and m-BCzCN in DCM at the mass ratios of 10:1–10000:1 and rapidly evaporating (60 °C) DCM solution, a series of host guest doping systems were constructed and optimized by using L-DCN and m-BCzCN as host and guest respectively. The results showed 1 % L-DCN/m-BCzCN (The mass ratio between L-DCN and m-BCzCN is 100:1) showed bright green afterglow by the switching on-off of 365 nm UV lamp, lasting for 5 s (Fig. S4 and Fig. 3). Furthermore, fluorescence maxima of 1 % L-DCN/m-BCzCN show red shifts of 35 nm compared with that of crystals L-DCN (Figs. 1c and 3b), which is close to that of 1 % m-BCzCN@PVA film (Fig. S3). Therefore, we can infer that fluorescence emission of 1 % L-DCN/m-BCzCN comes from m-BCzCN due to Förster energy transfer (FET) process from L-DCN to m-BCzCN [31,32]. Moreover, 1 % L-DCN/m-BCzCN yields multiple phosphorescence peaks at 500 nm, 540 nm, and 580 nm, with RTP lifetimes of 435.37 ms, 414.33 ms, and 360.49 ms, respectively, which is



**Scheme 1.** Synthesis procedures of DCN, L-DCN, and m-BCzCN.

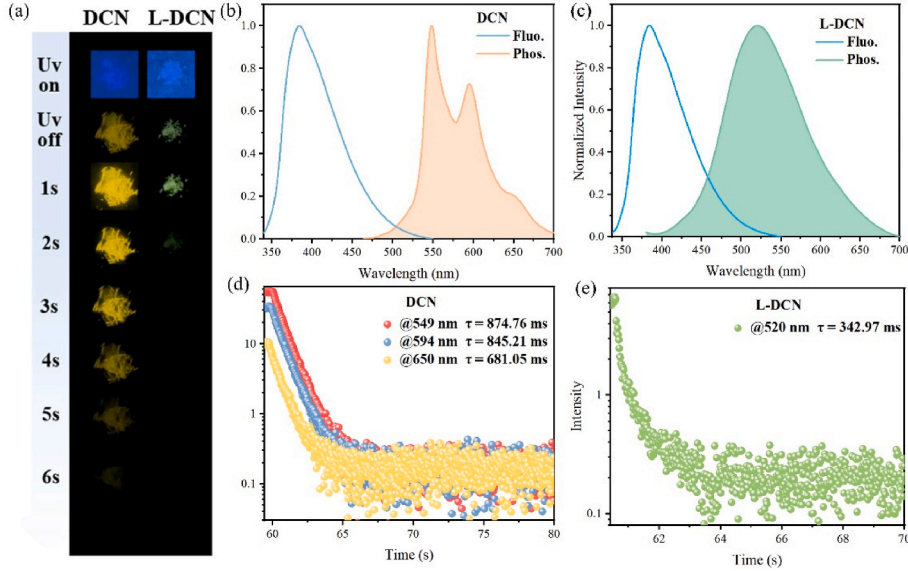


**Fig. 1.** (a) Photographs taken before and after irradiation with a 365 nm UV lamp. (b) Fluorescence and phosphorescent emission spectra of DCN and (c) L-DCN (delay time: 1 ms,  $\lambda_{\text{ex}}$ : 365 nm). (d) Time-resolved phosphorescent decay curves of DCN and (e) L-DCN ( $\lambda_{\text{ex}}$ : 365 nm).

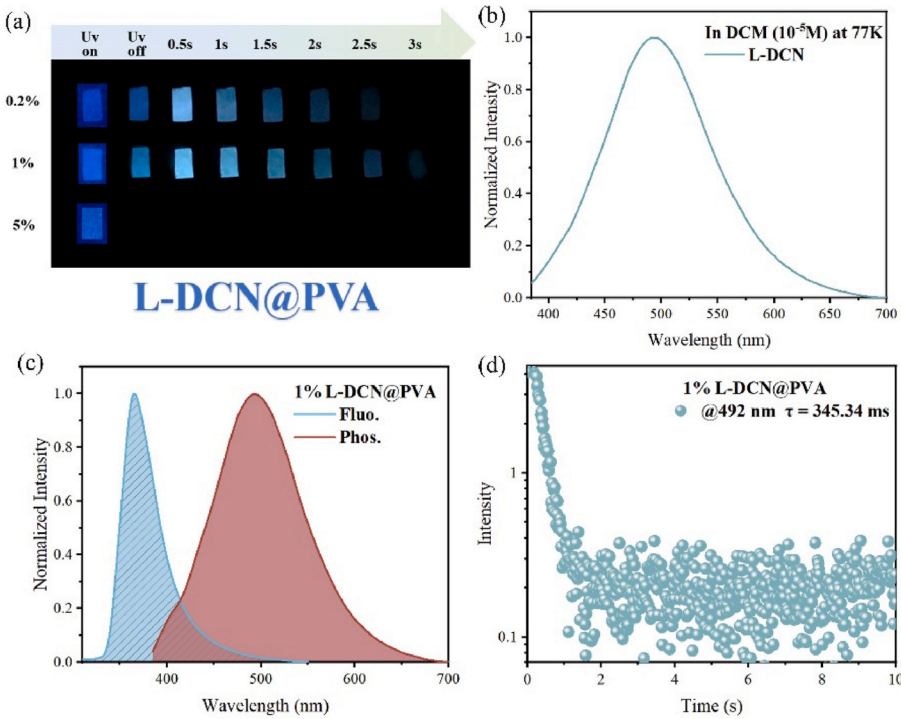


**Fig. 2.** (a) Photographs of L-DCN@PVA at different doping concentrations under a 365 nm UV lamp. (b) Phosphorescence spectra of L-DCN in DCM solution at 77 K ( $1 \times 10^{-5}$  M). (c) Fluorescence and phosphorescence emission spectra of 1 % L-DCN@PVA (delay time: 1 ms,  $\lambda_{\text{ex}}$ : 365 nm). (d) Time-resolved phosphorescent decay curve of 1 % L-DCN@PVA.

longer than that of crystals L-DCN and 1 % L-DCN@PVA (Fig. 3c). Of note, 1 % L-DCN/m-BCzCN and 1 % m-BCzCN@PVA film have almost identical RTP maxima (Fig. 3b and Fig. S3), which are also similar to that of m-BCzCN in DCM solution at 77 K (Fig. S3c). The results confirmed that RTP of 1 % L-DCN/m-BCzCN should be attributed to host sensitized guest emission. The excitation maxima of L-DCN and m-BCzCN are located at 350 nm and 270 nm, respectively (Fig. 3e). 1 % L-DCN/m-BCzCN emits bright green afterglow (5 s) by switching on/off 350 nm UV lamp, but without visible afterglow by switching on/off 270 nm UV lamp. (Fig. S5a). Furthermore, 1 % L-DCN/m-BCzCN shows

strong RTP intensity under excitation at 350 nm, but with weak RTP intensity under excitation at 270 nm (Fig. S5b). Thereby, the energy transfer between m-BCzCN and L-DCN is once again confirmed.

Subsequently, XRD spectra of crystals L-DCN, m-BCzCN, and 1 % L-DCN/m-BCzCN were investigated (Fig. 3f). Crystals L-DCN present strong XRD signals, demonstrating the ordered intermolecular arrangement and stacking, but without obvious XRD signal for m-BCzCN, indicating amorphous state, which should be the main reason of invisible afterglow for power m-BCzCN. 1 % L-DCN/m-BCzCN also show sharp XRD signals, and the main diffraction peaks are consistent with

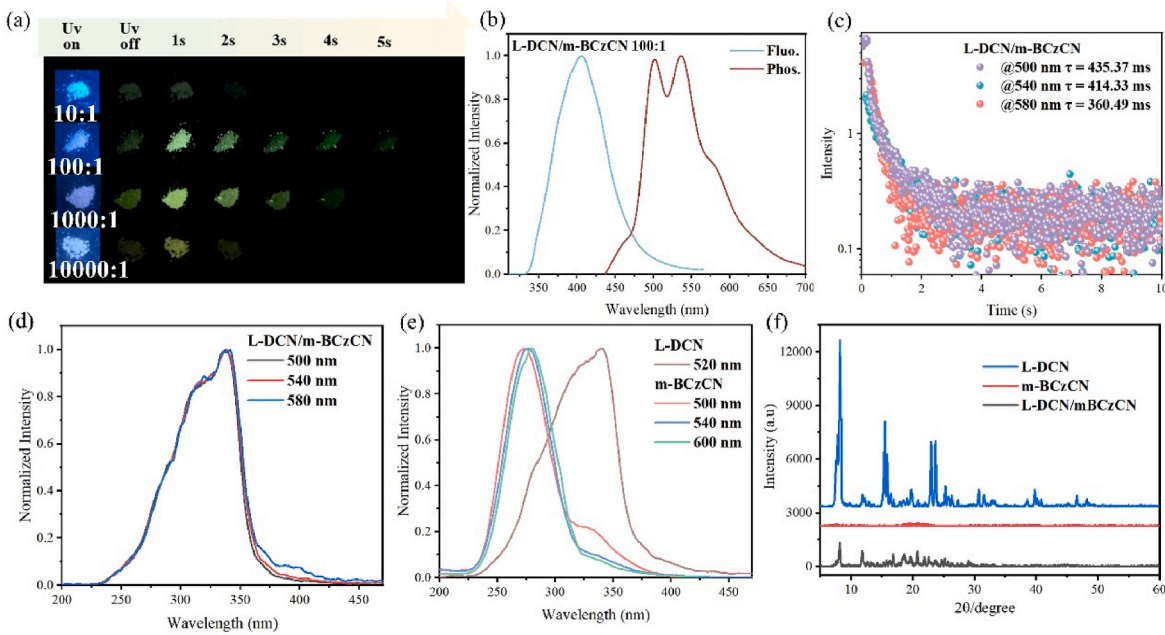


**Fig. 3.** (a) Photographs of L-DCN/m-BCzCN at different doping concentrations by the switching on-off of 365 nm UV lamp. (b) Fluorescence and phosphorescence emission spectra of 1 % L-DCN/m-BCzCN ( $\lambda_{\text{ex}}$ : 365 nm). (c) Time-resolved phosphorescence decay curves of 1 % L-DCN/m-BCzCN. (d) Excitation spectra of 1 % L-DCN/m-BCzCN at different emission peaks. (e) Phosphorescence excitation spectra of crystals L-DCN and m-BCzCN in DCM solution at 77 K. (f) X-ray diffraction patterns of crystals L-DCN, m-BCzCN and 1 % L-DCN/m-BCzCN.

crystals L-DCN, indicating excellent crystallinity for L-DCN. To study the intrinsic RTP mechanism of 1 % L-DCN/m-BCzCN, excitation spectra of crystals L-DCN, solid 1 % L-DCN/m-BCzCN, and m-BCzCN in DCM glassy solution (77 K) were measured and analyzed (Fig. 3d and e). Consistent with previous research results, 1 % L-DCN/m-BCzCN and crystal L-DCN exhibit similar excitation spectra, and excitation spectra of 1 % L-DCN/m-BCzCN at 500, 540 and 580 nm almost completely overlap [33–35]. Thereby, RTP of 1 % L-DCN/m-BCzCN was once again confirmed as L-DCN sensitized m-BCzCN luminescence, and different energy levels of 1 % L-DCN/m-BCzCN can mutually convert. In DCM glassy solution, m-BCzCN emits unimolecular phosphorescence, with shorter excitation maxima for m-BCzCN than crystals L-DCN, indicating that ordered molecular stacking can prolong molecular conjugation and excitation wavelength [36–39].

#### 2.4. Crystal analysis and theoretical Calculations

To further understand RTP, crystals DCN (CCDC 2055106) were obtained by slow solvent diffusion from n-hexane to DCM solution of DCN, with twisted molecular conformations (Fig. 4). There is no intermolecular  $\pi$ - $\pi$  stacking, and the dihedral angles of plane A1234-A14 N and A1234-B are  $5.44^\circ$  and  $75.51^\circ$  respectively, with multiple weak interactions such as C-H…C, C-H…N, and C-H… $\pi$ , and thereby rigidifying molecular configurations and suppressing non radiative deactivation of triplet excitons [40–43]. Molecular structures, the highest occupied molecular orbitals (HOMO) and the lowest unoccupied molecular orbitals (LUMO) distribution, energy level, and spin-orbit coupling constant ( $\xi$ ) between singlet and triplet states were optimized and achieved at the B3LYP/def2-SVP level. HOMO and LUMO of L-DCN simultaneously distributed on carbazole unit, for m-BCzCN concentrated on the benzocarbazole and benzene rings, indicating weak ICT effect (Fig. 4e). Moreover, HOMO and LUMO energy levels of m-BCzCN were embedded between HOMO and LUMO energy levels of L-DCN, confirming that FET can occur from L-DCN to m-BCzCN. Unimolecular L-DCN show weak ISC ability, only with two triplet excited states ( $T_4$  and  $T_5$ ) around the  $S_1$  state, corresponding to  $\xi(S_1 \rightarrow T_4)$  and  $\xi(S_1 \rightarrow T_5)$  of  $0.03 \text{ cm}^{-1}$  (Fig. 4f). As speculation, RTP crystals of L-DCN is mainly

attributed to more energy level splitting and intersystem transition channels in aggregated state. By contrast, m-BCzCN has small energy gaps (0.08 eV and 0.10 eV) between  $S_1$  and  $T_3$ ,  $T_2$ , as well as big  $\xi(S_1 \rightarrow T_2)$  and  $\xi(S_1 \rightarrow T_3)$ . Therefore, unimolecular m-BCzCN relative to unimolecular L-DCN can more easily generate triplet excitons, but poor crystallization ability leads to invisible RTP for solid m-BCzCN (Fig. 4g). Overall, the luminescence mechanism of 1 % L-DCN/m-BCzCN is that L-DCN transitions to the  $S_1$  state from ground state after absorbing energy under 365 nm UV radiation, which transfers energy to  $S_1$  state of m-BCzCN by FET process. Then, energy of  $S_1$  state transfers to  $T_2$  and  $T_3$  of m-BCzCN, then to  $T_1$  by ISC, vibration and relaxation. Finally,  $T_1$ -state excitons back to  $S_0$  state, emitting RTP of m-BCzCN. In the above process, good crystallization ability of L-DCN and compatibility between L-DCN and m-BCzCN are crucial for suppressing non radiative deactivation of m-BCzCN.

#### 2.5. Applications

L-DCN@PVA films with different doping concentrations display the same blue fluorescence and different afterglow lifetimes, which is conducive to construct high-level data encryption. As shown in Fig. 5, a set of data encryption was achieved by using 0.2 % L-DCN@PVA, 1 % L-DCN@PVA, and 5 % L-DCN@PVA films. Switching on a 365 nm UV lamp, number "8888" appeared, which became "0426" after creasing UV lamp radiation. After turning off the UV lamp for 3 s, number "0426" was replaced by number "0125".

#### 3. Conclusions

By introducing two CN groups via a  $\text{sp}^3$ -methylene linker, DCN, L-DCN and m-BCzCN were prepared, whose structures and purities were confirmed by  $^1\text{H}$  NMR and  $^{13}\text{C}$  NMR, HR-MS, X-ray single crystal diffraction, and HPLC. Crystals DCN show multiple RTP peaks, with  $\Phi_p$  of 14.7 and RTP lifetimes of 874.76 ms, while crystals L-DCN present single phosphorescence peak, with  $\Phi_p$  of 5.4 and RTP lifetimes of 342.97 ms, confirming phosphorescence nature of L-DCN and the important role of trace carbazole isomer. RTP performance of 1 % L-

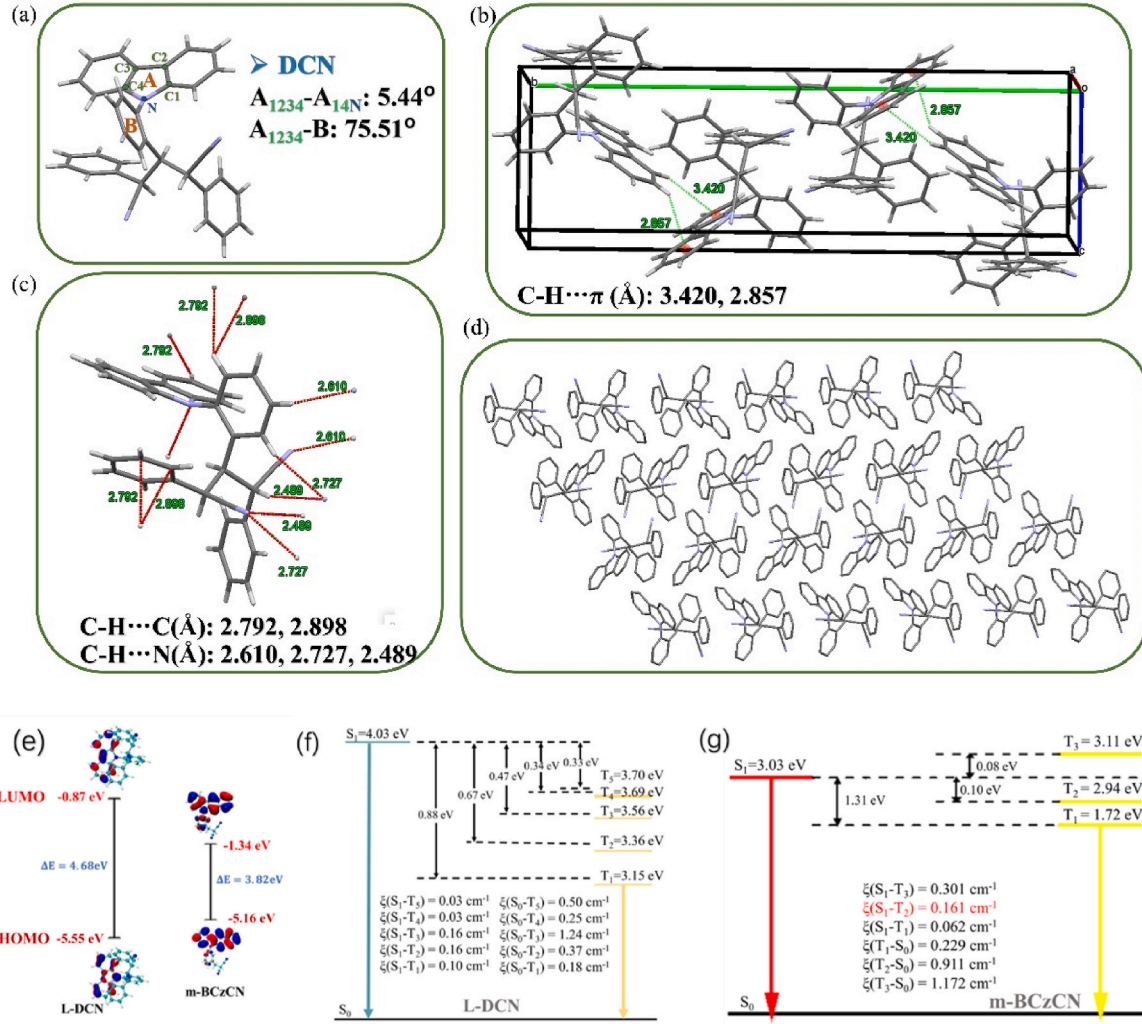


**Fig. 4.** (a) The spatial conformations of DCN. (b) Unit cell structures of DCN. (c) The intermolecular interactions of crystals DCN. (d) The intermolecular packing mode of DCN. (e) HOMO and LUMO distributions of L-DCN and m-BCzCN. (f) Energy levels and  $\xi$  of L-DCN and, (g) m-BCzCN.

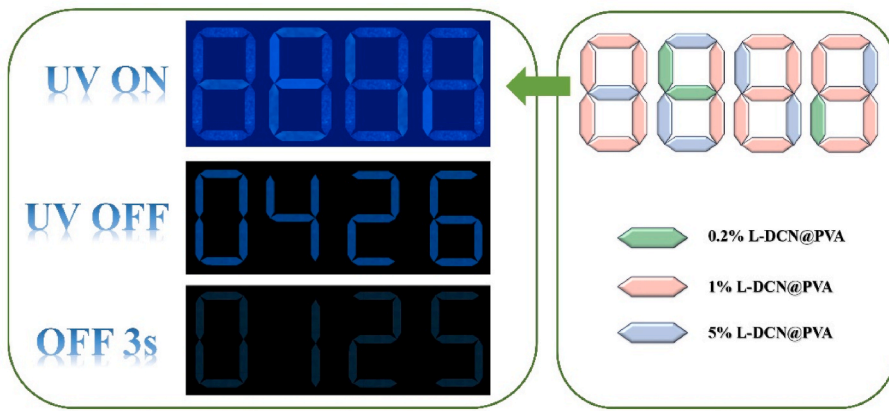


**Fig. 5.** Anti-counterfeiting application by using different L-DCN@PVA films.

DCN@PVA is not significantly improved, but 1 % L-DCN/m-BCzCN shows almost equivalent afterglow lifetime to crystals DCN due to good crystallization ability of L-DCN and compatibility between L-DCN and m-BCzCN. Phosphorescence spectra and XRD demonstrate that RTP of 1 % L-DCN/m-BCzCN are attributed to host sensitized guest emission. The work not only provides an efficient and simple construction method for

long-lived pure organic RTP materials by dissolution and rapid evaporation, as well as similar host and guest structures, but also contributes to boost high-level anti-counterfeiting application.

## CRediT authorship contribution statement

**Weirao Ji:** Writing – original draft, Data curation. **Yupeng Zhao:** Writing – review & editing, Software. **Jianmei Guo:** Writing – original draft, Investigation, Data curation. **Lei Ma:** Writing – review & editing, Software. **Yongtao Wang:** Writing – review & editing, Resources, Conceptualization.

## Declaration of competing interest

The authors declare that they have no known competing financial interests or personal relationships that could have appeared to influence the work reported in this paper.

## Acknowledgements

This work was supported by the Guangxi Natural Science Foundation (Grant No. 2024GXNSFAA010423 and 2020GXNSFAA159147), the National Natural Science Foundation of China (Grant No. 21766030 and 21566034) and the Guilin University of Technology Research Fund (Grant No. GUTQDJJ2019038 and GUTQDJJ2018052).

## Appendix A. Supplementary data

Supplementary data to this article can be found online at <https://doi.org/10.1016/j.optmat.2024.116416>.

5. The advanced encryptions were successfully constructed.

## Data availability

No data was used for the research described in the article.

## References

- [1] Y. Zhang, L. Chen, B. Liu, S. Yu, Y. Yang, X. Liu, Multicolor afterglow carbon dots: luminescence regulation, preparation, and application, *Adv. Funct. Mater.* (2024) 231536.
- [2] Z. Guan, Z. Tang, J. Deng, Y. Zheng, H. Li, X. Liu, Multi-color pure organic room temperature phosphorescent materials with long lifetime and high efficiency, *Adv. Funct. Mater.* 34 (2024) 2310198.
- [3] B. Fang, L. Lai, M. Fan, M. Yin, Designing organic room temperature phosphorescence with ultralong lifetime by substituent modification, *J. Mater. Chem. C* 9 (2021) 11172–11179.
- [4] H. Shi, W. Yao, W. Ye, H. Ma, W. Huang, Z. An, Ultralong organic phosphorescence: from material design to applications, *Acc. Chem. Res.* 55 (2022) 3445–3459.
- [5] S. Cai, X. Yao, H. Ma, H. Shi, Z. An, Manipulating intermolecular interactions for ultralong organic phosphorescence, *Aggregate* 4 (2023) e320.
- [6] G.-S. Zheng, C.-L. Shen, C.-Y. Niu, Q. Lou, T.-C. Jiang, P.-F. Li, X.-J. Shi, R.-W. Song, Y. Deng, C.-F. Lv, K.-K. Liu, J.-H. Zang, Z. Cheng, L. Dong, C.-X. Shan, Photooxidation triggered ultralong afterglow in carbon nanodots, *Nat. Commun.* 15 (2024) 2365.
- [7] Y. Su, S.Z.F. Phua, Y. Li, X. Zhou, D. Jana, G. Liu, W.Q. Lim, W.K. Ong, C. Yang, Y. Zhao, Ultralong room temperature phosphorescence from amorphous organic materials toward confidential information encryption and decryption, *Sci. Adv.* 4 (2018) eaas9732.
- [8] L. Gu, H. Shi, M. Gu, K. Ling, H. Ma, S. Cai, L. Song, C. Ma, H. Li, G. Xing, X. Hang, J. Li, Y. Gao, W. Yao, Z. Shuai, Z. An, X. Liu, W. Huang, Dynamic ultralong organic phosphorescence by photoactivation, *Angew. Chem. Int. Ed.* 57 (2018) 8425–8431.
- [9] T. Chen, L. Zheng, J. Yuan, Z. An, R. Chen, Y. Tao, H. Li, X. Xie, W. Huang, Understanding the control of singlet-triplet splitting for organic exciton manipulating: a combined theoretical and experimental approach, *Sci. Rep.* 5 (2015) 10923.
- [10] O. Bolton, K. Lee, H.-J. Kim, K.Y. Lin, J. Kim, Activating efficient phosphorescence from purely organic materials by crystal design, *Nat. Chem.* 3 (2011) 205–210.
- [11] G. Zhang, G.M. Palmer, M.W. Dewhirst, C.L. Fraser, A dual-emissive-materials design concept enables tumour hypoxia imaging, *Nat. Mater.* 8 (2009) 747–751.
- [12] Z.Y. Zhang, Y. Chen, Y. Liu, Efficient room-temperature phosphorescence of a solid-state supramolecule enhanced by cucurbituril, *Angew. Chem. Int. Ed.* 58 (2019) 6028–6032.
- [13] Z. Yang, Z. Mao, X. Zhang, D. Ou, Y. Mu, Y. Zhang, C. Zhao, S. Liu, Z. Chi, J. Xu, Y.-C. Wu, P.-Y. Lu, A. Lien, M.R. Bryce, Intermolecular electronic coupling of organic units for efficient persistent room-temperature phosphorescence, *Angew. Chem.* 128 (2016) 2221–2225.
- [14] Z. An, C. Zheng, Y. Tao, R. Chen, H. Shi, T. Chen, Z. Wang, H. Li, R. Deng, X. Liu, W. Huang, Stabilizing triplet excited states for ultralong organic phosphorescence, *Nat. Mater.* 14 (2015) 685–690.
- [15] B. Ding, X. Ma, H. Tian, Recent advances of pure organic room temperature phosphorescence based on functional polymers, *Acc. Mater. Res.* 4 (2023) 827–838.
- [16] Y. Wang, W. Liu, L. Ren, G. Ge, Deep insights into polymorphism initiated by exploring multicolor conversion materials, *Mater. Chem. Front.* 3 (2019) 1661–1670.
- [17] Y. Su, X. Jin, J. Su, Y. Feng, Q. Wang, Z. Zhang, H. Tian, X. Ma, Radical afterglow emission harnessed by doping N, N'-Diaryl-5,10-Dihydrophenazines to epoxy resins, *Adv. Opt. Mater.* 11 (2023) 2300604.
- [18] Y. Lei, W. Dai, Z. Liu, S. Guo, Z. Cai, J. Shi, X. Zheng, J. Zhi, B. Tong, Y. Dong, A novel strategy for realizing dual state fluorescence and low-temperature phosphorescence, *Mater. Chem. Front.* 3 (2019) 284–291.
- [19] J. Liu, J. Oliva, K. Tong, F. Zhao, D. Chen, Q. Pei, Multi-colored light-emitting electrochemical cells based on thermal activated delayed fluorescence host, *Sci. Rep.* 7 (2017) 1524.
- [20] C. Chen, K.C. Chong, Y. Pan, G. Qi, S. Xu, B. Liu, Revisiting carbazole: origin, impurity, and properties, *ACS materials letters*, *ACS Mater. Lett.* 3 (2021) 1081–1087.
- [21] C. Chen, Z. Chi, K.C. Chong, A.S. Batsanov, Z. Yang, Z. Mao, Z. Yang, B. Liu, Carbazole isomers induce ultralong organic phosphorescence, *Nat. Mater.* 20 (2021) 175–180.
- [22] J. Deng, Y. Bai, J. Li, J. Jiang, C. Zhao, W. Xie, Y. Guo, H. Liu, D. Liu, L. Yu, H. Wang, Yellow and orange-red room-temperature phosphorescence from amorphous nonaromatic polymers, *Adv. Opt. Mater.* 11 (2023) 2300715.
- [23] Y. Gong, J. Yang, M. Fang, Z. Li, Room-temperature phosphorescence from metal-free polymer-based materials, *Cell Reports Physiol. Sci.* 3 (2022) 100663.
- [24] H. Xiao, D.S. Zheng, L.Y. Zhang, L.J. Xu, Z.N. Chen, Ultra-long room temperature phosphorescence with the efficiency over 64% induced by 1‰ impurity doping, *Adv. Funct. Mater.* 33 (2023) 221424.
- [25] F.J. Hernández, R. Crespo-Otero, Excited state mechanisms in crystalline carbazole: the role of aggregation and isomeric defects, *J. Mater. Chem. C* 9 (2021) 11882–11892.
- [26] J. Guo, Y. Zhao, L. Ma, Y. Wang, Ultra-long room temperature phosphorescence, intrinsic mechanisms and application based on host-guest doping systems, *Chin. J. Struct. Chem.* (2024) 100335.
- [27] J.S. Yuan, Q. Sun, Y. Wang, L. Yue, J. Ma, Y. Zhang, H. Zhang, S. Xue, W. Yang, Manipulating matrix stacking modes for ultralong-duration organic room-temperature phosphorescence in trace isomer doping systems, *J. Mater. Chem. C* 9 (2021) 8302–8307.
- [28] J. Jiang, C. Hu, Y. Wang, L. Ma, J. Guo, Ultralong organic room-temperature phosphorescence, multiple stimulus responsiveness and high-level anti-counterfeiting based on multifunctional carbazolyl imidazolopyridine, *Mater. Today Chem.* 30 (2023) 2468–5194.
- [29] Z. Xie, X. Zhang, H. Wang, C. Huang, H. Sun, M. Dong, L. Ji, Z. An, T. Yu, W. Huang, Wide-range lifetime-tunable and responsive ultralong organic phosphorescent multi-host/guest system, *Nat. Commun.* 12 (2021) 3522.
- [30] J. Guo, C. Hu, J. Liu, Y. Wang, L. Ma, Mechanochromism, tunable pure organic room temperature phosphorescence, single-molecule near-white emission, digital encryption, and anti-counterfeiting, *Dyes Pigments* 221 (2024) 111760.
- [31] Q. Wang, L. Chen, Q. Yang, Y. Xu, H. Wang, Z. Xie, Efficient solution-processed red fluorescent oleds using diluted duplex host to reduce non-radiative loss of triplet excitons, *Adv. Mater. Interfac.* (2022) 2200830.
- [32] S. Shen, G.V. Baryshnikov, Q. Xie, B. Wu, M. Lv, H. Sun, Z. Li, H. Ågren, J. Chen, L. Zhu, Making multi-twisted lumiphores produce persistent room-temperature phosphorescence, *Chem. Sci.* 14 (2023) 970–978.
- [33] J. Jiang, J. Liu, C. Hu, Y. Wang, L. Ma, Construction and fine tuning of host-guest doping systems and the underlying mechanism of room temperature phosphorescence, *Dyes Pigments* 222 (2024) 111931.
- [34] J. Jiang, Y. Wang, L. Ma, X. Li, X. Wang, Y. Guo, Aie activity, mechanochromic property and solvent inclusion of two B-diketones with tetraphenylethylene unit, *Tetrahedron* 136 (2023) 133355.
- [35] J. Guo, J. Liu, Y. Zhao, Y. Wang, L. Ma, J. Jiang, Time-dependent and clustering-induced phosphorescence, mechanochromism, structural-function relationships, and advanced information encryption based on isomeric effects and host-guest doping, *Spectrochim. Acta* 317 (2024) 124449.
- [36] C. Sun, X. Ran, X. Wang, Z. Cheng, Q. Wu, S. Cai, L. Gu, N. Gan, H. Shi, Z. An, H. Shi, W. Huang, Twisted molecular structure on tuning ultralong organic phosphorescence, *J. Phys. Chem. Lett.* 9 (2018) 335–339.
- [37] X. Zhang, D. Wang, H. Shen, S. Wang, Y. Zhou, Y. Lei, W. Gao, M. Liu, X. Huang, H. Wu, 3,6-Diamino-7,8-Dihydroisoquinoline-4-Carbonitrile derivatives: unexpected facile synthesis, full-color-tunable solid-state emissions and mechanofluorochromic activities, *Org. Chem. Front.* 8 (2021) 856–867.
- [38] Y. Li, L. Jiang, W. Liu, S. Xu, T.-Y. Li, F. Fries, O. Zeika, Y. Zou, C. Ramanan, S. Lenk, R. Scholz, D. Andrienko, X. Feng, K. Leo, S. Reineke, Reduced intrinsic non-radiative losses allow room-temperature triplet emission from purely organic emitters, *Adv. Mater.* 33 (2021) 2101844.
- [39] Y. Yang, Y. Liu, Y. Liu, K. Jiang, Structure-lock induced phosphorescence lifetime enhancing of (9h-carbazol-9-yl) (phenyl) methanone: an organic phosphorescent materials, *J. Lumin.* 227 (2020) 117587.
- [40] Y. Li, L. Jiang, W. Liu, S. Xu, T.-Y. Li, F. Fries, O. Zeika, Y. Zou, C. Ramanan, S. Lenk, R. Scholz, D. Andrienko, X. Feng, K. Leo, S. Reineke, Reduced intrinsic non-radiative losses allow room-temperature triplet emission from purely organic emitters, *Adv. Mater.* 33 (2021) 2101844.

- [41] J. Chen, X. Chen, L. Cao, H. Deng, Z. Chi, B. Liu, Synergistic generation and accumulation of triplet excitons for efficient ultralong organic phosphorescence, *Angew. Chem.* 134 (2022) e202200343.
- [42] A.C. Brannan, N.L. Phuoc, M. Linnolahti, A.S. Romanov, Organic persistent room temperature phosphorescence enabled by carbazole impurity, *Front. Chem.* 10 (2023) 1008658.
- [43] F. Martínez-Lara, A. Suárez, S. Suárez-Pantiga, M.J. Tapia, R. Sanz, Straight access to highly fluorescent angular indolocarbazoles via merging Au- and Mo-catalysis, *Org. Chem. Front.* 7 (2020) 1869–1877.